POLITECNICO DI TORINO
Repository ISTITUZIONALE

NonLinear Influence of Reservoir Initial Condition on Flood Reduction

*Original*
NonLinear Influence of Reservoir Initial Condition on Flood Reduction / Evangelista, G., Bertola, M., Blöschl, G., Claps, P.. - In: JOURNAL OF FLOOD RISK MANAGEMENT. - ISSN 1753-318X. - 18:4(2025), pp. 1-16. [10.1111/jfr3.70142]

*Availability:*
This version is available at: 11583/3004293 since: 2025-10-21T09:04:08Z

*Publisher:*
Wiley

*Published*
DOI:10.1111/jfr3.70142

*Terms of use:*

This article is made available under terms and conditions as specified in the corresponding bibliographic description in the repository

*Publisher copyright*

(Article begins on next page)

16 November 2026

Check for updates

*Journal of Flood Risk Management*

WILEY

CIWEM Chartered Institution of Water and Environmental Management | Journal of Flood Risk Management

ORIGINAL ARTICLE OPEN ACCESS

# Non-Linear Influence of Reservoir Initial Condition on Flood Reduction

Giulia Evangelista[1] | Miriam Bertola[2] | Günter Blöschl[2,3] | Pierluigi Claps[1]

[1]Department of Environment, Land and Infrastructure Engineering, Politecnico di Torino, Torino, Italy | [2]Institute of Hydraulic Engineering and Water Resources Management, Technische Universität Wien, Vienna, Austria | [3]Department of Civil, Chemical, Environmental, and Materials Engineering, Università di Bologna, Bologna, Italy

**Correspondence:** Giulia Evangelista (giulia.evangelista@polito.it)

**Received:** 22 May 2025 | **Revised:** 21 September 2025 | **Accepted:** 9 October 2025

**Funding:** This study was supported by European Union Next-GenerationEU (National Recovery and Resilience Plan—NRRP, Mission 4, Component 2, Investment 1.3-D.D. 1243 2/8/2022, PE0000005-Spoke TS 2).

**Keywords:** flood control | flood peak reduction | flood risk | initial reservoir storage | reservoir

## ABSTRACT

Reservoirs play a crucial role in modifying natural flow regimes and mitigating flood peaks, yet their effectiveness depends heavily on operational strategies, particularly the initial storage level at the onset of a flood event. This study investigates, for the first time, the non-linear effects of reduced initial storage on the relationship between flood peak attenuation efficiency and flood return period for about 250 large dams in Italy. We estimate flood hydrographs via a simplified hydrological model and apply full hydraulic routing under different scenarios of initial reservoir storage, informed by historical reservoir time series and regional flood seasonality. Our findings reveal that flood peak attenuation is highly sensitive to the initial storage level, with dam performance deteriorating sharply as flood return periods increase, especially when initial storage is high. Seven distinct classes of dams are identified based on their flood attenuation capacity relative to flood severity, highlighting non-linear and threshold effects that are often overlooked in regional dam safety assessments. Notably, the commonly assumed full-reservoir condition yields overly conservative estimates: under this assumption, approximately 20% of the dams reach their maximum allowed water level for return periods of 100 years or less. This national-scale analysis provides new insights into regional differences in reservoir operation, particularly between hydropower-oriented dams in the Alps and water supply reservoirs in southern Italy. By explicitly quantifying how reduced initial storage can enhance flood mitigation, the study offers practical recommendations for optimizing reservoir operations under current and future climatic conditions.

## 1 | Introduction

Natural flow regimes are significantly modified by artificial reservoirs and dams (Hall et al. 2014; Brunner 2021; Salwey et al. 2023; Bai et al. 2024), with the extent of these changes largely dependent on the operational strategies and management practices implemented. One way to quantify dam-induced flow changes involves analyzing pre- and post-dam streamflow data (e.g., Wang et al. 2017; Zhao et al. 2020; Stecher and Herrnegger 2022). When hydrological data at the dam site is not available, flow alterations induced by dams, particularly during flood events, are investigated through modeling approaches, which often combine a rainfall-runoff model with a reservoir routing module to estimate discharges at the reservoir outlet (e.g., Sordo-Ward et al. 2012; Volpi et al. 2018; Antolini and Tate 2021; Evangelista et al. 2023).

This is an open access article under the terms of the Creative Commons Attribution License, which permits use, distribution and reproduction in any medium, provided the original work is properly cited.

© 2025 The Author(s). *Journal of Flood Risk Management* published by Chartered Institution of Water and Environmental Management and John Wiley & Sons Ltd.

The complexity of modeling reservoir routing during floods varies based on the specific goals of the study, ranging from simplified assumptions to highly detailed analyses incorporating local data.

The standard engineering practice for the assessment of flood attenuation assumes a constant initial water level at full reservoir capacity (Federal Emergency Management Agency (FEMA) 2012), that is, the initial water level corresponds to the spillway crest elevation. This assumption is adopted as a conservative measure in hydrological safety analyses, as it corresponds to the worst situation for flood attenuation. However, reservoir levels can vary considerably due to seasonal or operational factors, and the initial water level in the reservoir, that is, the level at which flood routing begins, is a critical variable influencing flood alteration by dams (Carvajal et al. 2009; Micovic et al. 2016; Gabriel-Martin et al. 2017). While seasonal variability is generally predictable, operational fluctuations often stem from undocumented decision-making processes, as water release schedules are governed by competing objectives such as water supply, hydropower generation, irrigation demands, and flood control. This variability is particularly pronounced in hydropower reservoirs, which often undergo rapid and frequent fluctuations as operators may adjust water levels to meet energy production schedules. Based on such variability, rare floods may occur when the reservoir is only partially filled, allowing some of the inflow to be stored. It may equally be possible for a flood to arrive when the reservoir level exceeds a normal (non-full capacity) operating level. In this context, it would be helpful for dam operators to have quantitative indications of whether the available volume at a given time of the year is sufficient to manage a given flood event.

In Italy, specific regulations, such as the Prime Minister's Directive of 8 July 2014 ("Operational guidelines related to civil protection activities in catchments containing large dams"), allow for the allocation of empty storage volumes during certain periods to make a storage capacity available for flood attenuation and reduce downstream hydraulic risk. Furthermore, it is noteworthy that approximately 30% of Italian dams operate under limited or experimental conditions while awaiting functional and technical testing, a situation particularly pronounced in regions such as Sardinia, Sicily, Calabria, and Basilicata (Evangelista et al. 2025). Lastly, the storage state of reservoirs in Italy over the past 5 years has been heavily impacted by prolonged droughts, particularly in southern regions. Reduced inflows have left many reservoirs nearly dry, a condition that studies suggest may become more frequent in the future due to climate change (e.g., Liuzzo et al. 2015; Peres et al. 2019). All these considerations suggest that the assumption of a reservoir being at full capacity when a flood occurs, while conservative, is an uncommon scenario.

A lowered water level introduces significant changes to flood routing dynamics. When a reservoir is full at the start of a flood event, its flood peak attenuation potential becomes highly constrained, as the storage capacity has already been almost exhausted. In such scenario, any further inflow contributes directly to an increase in water level, which determines the outflow through spillways. This condition leads the attenuation capacity to be primarily governed by the reservoir surface area (Sordo-Ward et al. 2012; Evangelista et al. 2023): the larger the lake area, the more pronounced the attenuation effect will be (at least for similar hydraulic conditions of the spillways). When the initial storage in a reservoir is below its maximum capacity, flood attenuation is affected by the structure's non-linear behavior, fundamentally altering its efficiency in mitigating flood peaks. This nonlinearity arises from the increased availability of storage capacity, which enables a significant portion of the inflow to be temporarily retained in the reservoir before the water level reaches the spillway elevation. The extent of nonlinearity is controlled by factors such as the reservoir's geometry, that is, the way storage volume changes with elevation. In essence, reservoirs exhibit a threshold effect: small inflows may be entirely stored without any increase in outflow, while larger inflows result in a progressively dampened response as the reservoir approaches its maximum capacity.

Existing studies have focused on the influence of initial water levels on dam safety assessment (e.g., Micovic et al. 2016; Gabriel-Martin et al. 2017, 2019; Lu et al. 2022; Lompi et al. 2023; Brigandì et al. 2023). Gabriel-Martin et al. (2019), in particular, investigated the impact of initial reservoir levels on hydrological dam safety using a Monte Carlo method applied to a Spanish reservoir. Their study compared three scenarios with varying initial levels and a huge number of simulated flood hydrographs. The results, assessed using a risk index, underscore the importance of accounting for initial level variability for a more accurate hydraulic risk assessment. Similarly, Micovic et al. (2016) used a Monte Carlo approach to show that dam overtopping is more likely to be caused by a combination of a smaller flood and a system component failure than by an extreme flood alone. Most of the above contributions, however, have focused on single case studies or on synthetic reservoir configurations, which limit the general validity of their findings. Furthermore, none have explicitly examined the nonlinear effects introduced by reduced initial storage levels on the relationship between the attenuation efficiency and the flood return period.

To address this gap, this work explores the relationship between flood return period and flood peak attenuation for over 200 real reservoirs in Italy. The variability of the attenuation effect is examined as a function of the ratio between flood volume and available storage capacity, taking into account seasonal fluctuations in reservoir storage and their interaction with the seasonal patterns of flood events. This analysis is supported by historical time series of reservoir storage from approximately 70 reservoirs across the country. In Italy, like in many other countries, reservoir storage records are very rarely made available, making this collection of historical reservoir data an additional, original contribution to this research.

To allow an assessment on such a large scale, we have adopted a simple hydrological scheme for the design hydrograph and a "no gates management" approach, yet using a full hydraulic routing, as done in a previous evaluation of flood attenuation potentials performed by the authors (Evangelista et al. 2023). With respect to this previous approach, this work quantifies dam efficiency more rigorously, surpassing ranking-based evaluations: some simplifying assumptions, such as constant



1753318x, 2025, 4, Downloaded from https://onlinelibrary.wiley.com/doi/10.1111/jfr3.70142 by Politecnico Di Torino Sist. Bibl Del Polit Di Torino, Wiley Online Library on [21/10/2025]. See the Terms and Conditions (https://onlinelibrary.wiley.com/terms-and-conditions) on Wiley Online Library for rules of use; OA articles are governed by the applicable Creative Commons License

full-lake scenarios and simplified spillway representations, are relaxed, and non-linear flood reduction dynamics are explicitly explored, to reach results closer to actual operational configurations. This analysis can hence provide a useful framework for evaluating potential reduction in dam efficiency as flood severity increases, both under current climate conditions and in future scenarios. Indeed, reservoir water levels are expected to vary because of increased potential evapotranspiration and reduced snow storage, as shown in a review paper by Fluixá-Sanmartín et al. (2018).

The findings of this study can offer helpful insights for dam managers on the effectiveness of maintaining unfilled storage capacity for flood mitigation: by quantifying the impact of initial reservoir storage on flood attenuation, this research provides a data-driven basis for optimizing reservoir operations, particularly in balancing water storage needs with flood risk management. For instance, notable differences can be recognized between reservoirs in the Alpine region, primarily used for hydropower generation, and those in southern Italy, which serve mainly for irrigation and drinking water supply.

The methodology is detailed in Section 2, and the data sources are described in Section 3. Sections 4 and 5 present the results of the analysis and their discussion. For the sake of brevity, more in-depth, site-specific considerations on three selected dams, representative of the Italian context, can be found in Appendix A.

## 2 | Methods

### 2.1 | Determination of Reservoir Inflow Hydrographs

Inflow hydrographs are characterized in terms of their peak and shape. To estimate incoming flood peaks, we apply the rational formula, as defined in Equation (1):

$$Q_T = \frac{C\, i(d_c, T) A_B}{3,6} \tag{1}$$

where $A_B$ is the basin area (km$^2$), $i(d_c,T)$ is the estimated extreme rainfall intensity (mm/h) for a critical duration $d_c$ and a return period $T$, and $C$ is the runoff coefficient (dimensionless). The critical duration $d_c$ can be considered equal to the basin time of concentration $t_c$. According to the index-flood approach, the design rainfall intensity quantile can be expressed by means of the Intensity-Duration-Frequency (IDF) curves, which are defined as:

$$i(t_c, T) = \frac{h(t_c, T)}{t_c} = K_T \cdot a \cdot t_c^{n-1} \tag{2}$$

where $h(t_c,T)$ is the quantile of the annual maximum rainfall depth for the duration $t_c$ and the return period $T$, $a$ and $n$ are the scale factor and the scaling exponent, respectively, and $K_T$ is the "non dimensional inverse frequency factor", also called "growth factor". A fixed set of return periods, ranging from 5 to 10,000 years, is considered, while catchment-averaged values for $a$, $n$ and $K_T$ are computed as described in Evangelista et al. (2023).

To account for different hydrological forcings, two values for the runoff coefficient, $C=0.5$ and $C=1$, are considered. The time of concentration $t_c$ is computed based on considerations of reasonable, catchment-averaged values of flow velocities, following the methodology proposed by Evangelista et al. (2024), as shown in Equation (3):

$$t_c = \frac{L_{LDP}}{v} \tag{3}$$

where $L_{LDP}$ is the length of the longest drainage path and $v$ is the mean travel velocity. The determination of $v$ depends on the basin size. For basins smaller than 200 km$^2$, $v$ is calculated by rearranging Equation (3) and substituting $t_c$ with the value given by the Watt and Chow formula (Watt and Chow 1985). For basins bigger than 200 km$^2$, $v$ is obtained similarly, but $t_c$ is replaced by the value from the NERC formula (Natural Environment Research Council (NERC) 1975). This approach ensures that estimates of $t_c$ are based on something physically meaningful, such as flow velocities, and that these velocities are properly scaled to the characteristics of the catchment. As for the hydrograph shape, a simple, triangular hydrograph is adopted, with duration $D=2t_c$.

We recognize that these choices may appear oversimplified, particularly considering that the effectiveness of flood mitigation is highly sensitive to both the magnitude of the incoming flood volume and the hydrograph shape, as well as the hydrograph duration (Zhao et al. 2020; Manfreda et al. 2021; Evangelista et al. 2023). However, the main goal of this study is not to quantify value ranges of flood attenuation for large Italian dams, but rather to investigate how the attenuation effect varies as flood severity increases. In this context, the rational formula is employed to take advantage of the latest and state-of-the-art data on rainfall extremes in the catchment areas upstream of these dams, as will be detailed in Section 3. Hydrograph shapes (and volumes), on the other hand, are intentionally kept as simple as possible. In an effort to disconnect the analysis from specific hydrograph characteristics, the discussion section explores how the attenuation depends on hydrological forcings expressed in terms of dimensionless quantities. This approach will facilitate a more generalized interpretation of the results.

### 2.2 | Estimation of Initial Storage Levels

Initial reservoir storage prior to a flood, assuming the reservoir is not at full capacity, is determined by combining two pieces of information: (i) the average seasonal timing of floods and (ii) the variability of the reservoir storage throughout the year, as depicted in Figure 1.

Regarding point (i), the average day of the year on which the 10 most extreme floods occurred between 1960 and 2020 was calculated for over 400 gauged sites across Italy, using the methodology described in Blöschl et al. (2017). For each gauge, we considered the dates of occurrence of the selected events in any



1753318x, 2025, 4, Downloaded from https://onlinelibrary.wiley.com/doi/10.1111/jfr3.70142 by Politecnico Di Torino Sist. Bibl Del Polit Di Torino, Wiley Online Library on [21/10/2025]. See the Terms and Conditions (https://onlinelibrary.wiley.com/terms-and-conditions) on Wiley Online Library for rules of use; OA articles are governed by the applicable Creative Commons License

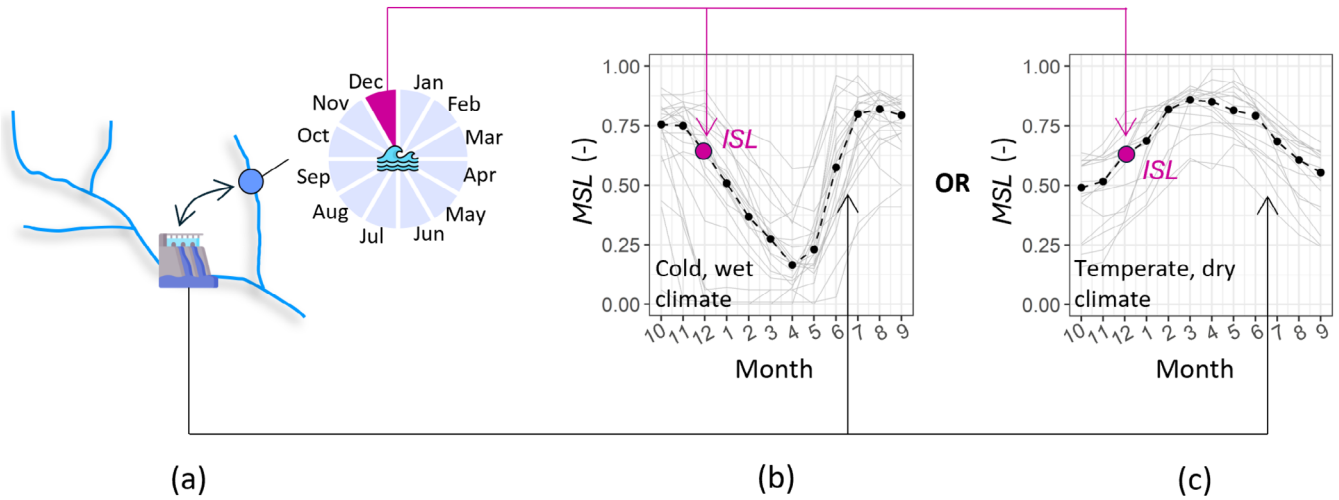



**FIGURE 1** | Reconstruction of the initial reservoir storage level (*ISL*) based on regional flood seasonality. The average month of flood occurrence is assigned to each dam based on data from the nearest gauged site (a). The *ISL* is identified along the annual curve of the median reservoir storage level (*MSL*, dashed black line), which is derived for each dam by generalizing observed reservoir storage level data (thin gray lines). Curves are shown for dams in wet, cold climates (b) and temperate, dry climates (c). *MSL* and *ISL* are computed according to Equations (4) and (5), respectively. Panel (a) has been designed using resources from Flaticon.com.

calendar year. The average day of flood occurrence was determined by expressing each date as an angular value and computing the circular mean. The mean length of the flood series is 25.9 years over the period considered, with a minimum of 11 years and a maximum of 61 years. Although the gauging stations are not located at the dam sites analyzed, each reservoir was matched to the average flood timing of the nearest gauge (Figure 1a). This correspondence is considered plausible due to the relatively short distances between dams and the associated gauges; the largest recorded distance is approximately 40 km, found in the Alpine region, where the gauge network is less dense.

As for point (ii), observed measurements of reservoir storage levels from a representative sample of Italian dams were carefully collected and analyzed. Dams in both northern and southern Italy, including islands, have been considered to account for the great variability in both climatic conditions and reservoir purposes across Italy. Specifically, reservoir storage data for dams in Piedmont, Aosta Valley, and Sardinia were retrieved. The collected data were used to compute the empirical monthly median storage level (hereinafter *MSL*) throughout the year, according to Equation (4):

$$MSL = \frac{V}{V_{aut}} \tag{4}$$

where $V$ and $V_{aut}$ are the actual stored volume and the maximum authorized storage volume, respectively. *MSL* can vary between 0 and 1 and has to be understood as a portion of the reservoir's authorized storage volume that is filled at any given month during the year.

A criterion is needed to generalize the information to estimate the *MSL* values for dams where historical observations are unavailable. The analysis of reservoirs in Piedmont, Aosta Valley, and Sardinia has revealed elevation-dependent storage and release cycles. High-elevation reservoirs exhibit pronounced seasonal variability, characterized by strong accumulation during snowmelt periods. In contrast, low-elevation reservoirs present negligible seasonal fluctuations. These findings are consistent with the observations of Brunner and Naveau (2023) for reservoirs in the central Alps.

For this reason, an empirical classification criterion was developed to quantify the variability of the median storage level throughout the year, based on (i) dam elevation and (ii) regional climatology. Here the Köppen-Geiger climate classification (Beck et al. 2023) was used. Based on this criterion, two distinct dam categories were defined (Figure 1b,c): dams located at elevations above 1400 m a.s.l., predominantly within cold and humid climatic zones according to the 1991–2020 Köppen-Geiger climate classification map, and non-Alpine dams, located below 1400 m a.s.l., in areas with temperate and generally dry climates. In Figure 1b,c, thin gray lines show the *MSL* values computed for each dam in each month, while dashed black lines represent the median *MSL* values over all dams. Snow-dominated regions such as the Alps exhibit the highest reservoir storage levels during the summer months (Figure 1b). This is consistent with the typical runoff seasonality of basins in snowmelt-dominated environments. In drier and in irrigation-dominated regions, typically in southern Italy, reservoirs tend to maintain higher storage levels year-round (Figure 1c). These reservoirs store more water during winter and gradually deplete in summer, reaching their lowest levels in October, aligned with the end of the irrigation season. By applying the criterion outlined above, an annual *MSL* pattern could be assigned to each of the dams considered. From this, we identified the month on the annual *MSL* curve when, on average, the highest floods occur at each dam, allowing us to define an initial storage level (*ISL*), as shown in Figure 1. The *ISL* , which serves as the initial condition for dam routing, is defined in a way consistent to Equation (4) as follows:

$$ISL = \frac{V_{initial}}{V_{aut}} \tag{5}$$



1753318x, 2025, 4, Downloaded from https://onlinelibrary.wiley.com/doi/10.1111/jfr3.70142 by Politecnico Di Torino Sist. Bibl Del Polit Di Torino, Wiley Online Library on [21/10/2025]. See the Terms and Conditions (https://onlinelibrary.wiley.com/terms-and-conditions) on Wiley Online Library for rules of use; OA articles are governed by the applicable Creative Commons License

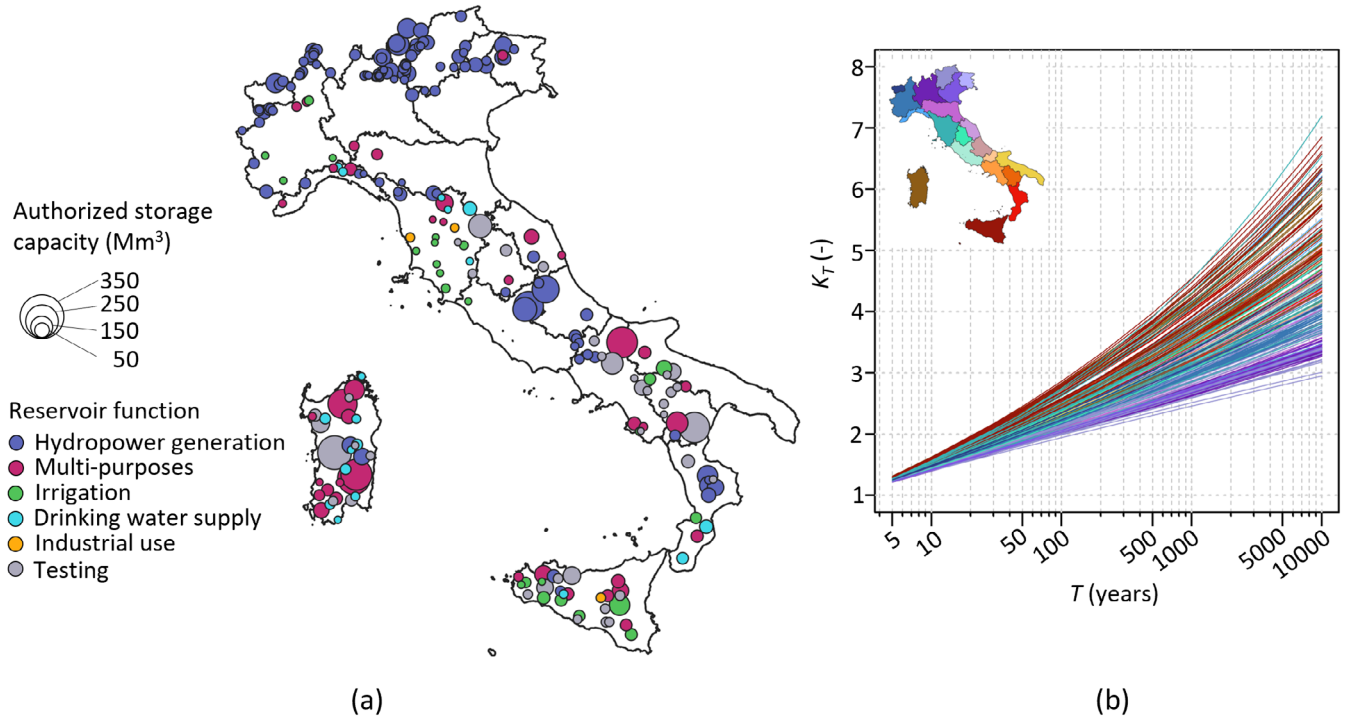



**FIGURE 2** | Distribution of the 247 dams categorized by purpose and authorized storage capacity (a). Catchment averaged values of rainfall growth factors $K_T$ for upstream basins, shown as a function of rainfall return periods and classified by Italian regions (b).

where $V_{initial}$ is the initial stored volume.

In a second scenario considered in this study, *ISL* is set to 1, meaning that the reservoir is assumed to be full at the onset of a flood event.

### 2.3 | Dam Routing

The flood peak attenuation performed by a reservoir is assessed by solving the continuity equation of lakes:

$$q_i(t) - q_o(h(t)) = \frac{dV(h(t))}{dt} \quad (6)$$

where $q_i(t)$ and $q_o(t)$ are the inflow and outflow discharges respectively, $V$ is the reservoir volume and $h$ is the water level above the spillway crest. Once Equation (6) is solved for $q_o(t)$, the attenuation coefficient $\eta$, which varies between 0 and 1, is defined as the ratio of the outgoing and the incoming peak discharges. For each basin, the attenuation coefficient is obtained for each return period considered. This analysis considers only free-surface spillways, assuming that gates-controlled spillways operate with their gates fully open. This assumption is justified by the distribution of spillway types across Italian dams: approximately 75% of them are equipped with free spillways or spillways with radial gates, both of which are designed to operate under free-flow conditions. The remaining 25% is almost evenly divided between spillways with vertical rising gates, rising sector gates, and mixed spillways (a combination of free and controlled spillways). Consequently, 75% of the spillways at large Italian dams operate without active supervision.

The outflow discharge $q_o(t)$ dependence on the spillway's geometric features is assumed to be constant, with the Creager law applied to all spillways. For dams with multiple spillways at the same elevation, their lengths have been merged. In the case of several spillways located at different levels, unlike in Evangelista et al. (2023), where only the highest one was considered to solve Equation (6), this study considers each spillway at its actual elevation.

As mentioned in the previous section, two scenarios for the *ISL* in the reservoir are considered. When *ISL* equals 1, that is, when the initial water level is equal to the spillway crest elevation, spillways start working at $t=0$, and the rise in level $dh(t)$ in Equation (6) is determined by the ratio between $dV(h(t))$ and the (constant) lake area. However, if the reservoir is not full at $t=0$, estimating a starting water level from the *ISL* would require knowing the reservoir's volume curve. Since stage-storage curves are not available for all dams, Equation (6) is dealt with to track the increase in volume over time, rather than the increase in water level, until the reservoir reaches full capacity. When this occurs, we switch to tracking water levels rather than volume changes.

## 3 | Data

### 3.1 | Italian Large Dams and Upstream Catchments

The present analysis is carried out on 247 reservoirs all over Italy (Figure 2a). This sample was selected through a screening process that excluded the following cases:

i. Dams that have been officially decommissioned;



1753318x, 2025, 4, Downloaded from https://onlinelibrary.wiley.com/doi/10.1111/jfr3.70142 by Politecnico Di Torino Sist. Bibl Del Polit Di Torino, Wiley Online Library on [21/10/2025]. See the Terms and Conditions (https://onlinelibrary.wiley.com/terms-and-conditions) on Wiley Online Library for rules of use; OA articles are governed by the applicable Creative Commons License

ii. Dams already used for flood control purposes;

iii. Dams where no attenuation volume is available or no unsupervised management is possible (this applies particularly on structures regulating large natural lakes);

iv. Dams with very small lake areas $A_L$ in relation to the upstream watershed area $A_B$ (ratios $A_L/A_B$ lower than 1/150).

v. Dams for which information on spillway geometry is under review due to ongoing dimensional adjustments.

Structural features of the dams, including reservoir volumes, lake areas, and elevation characteristics, are retrieved from TILDE (The Italian Large Dams datasEt, Evangelista et al. 2025), while information on spillway geometries is provided by the Italian Department of Dams. Similarly, upstream catchment attributes required to estimate incoming flood peaks, such as catchment areas, characteristic lengths and slopes, and extreme rainfall-related attributes based on a Generalized Extreme Value (GEV) distribution, are also sourced from Evangelista et al. (2025). Figure 2b shows curves of catchment-averaged values of the growth factor $K_T$ of Equation (2) with return periods for the catchments upstream of the 247 dams.

As mentioned in the introduction, many reservoirs in Italy are currently operating outside their normal conditions. This means that, in these cases, water levels are lowered, resulting in a reduction in the authorized storage volumes. For better understanding, Figure 3 illustrates the ratio of the authorized volume $V_{aut}$ to the total volume at the spillway elevation $V_s$, in relation to the difference between the spillway elevation $H_s$ and the maximum authorized water level $H_{aut}$ for dams under different operating conditions. In some cases, authorized water levels are lowered by more than 10 m, leading to a reduction of up to 50% in the total storage capacity. Since the volume stored at the onset of the flood is considered a fraction of the authorized volume (see Equation (5)), this condition influences the estimation of the *ISL*.

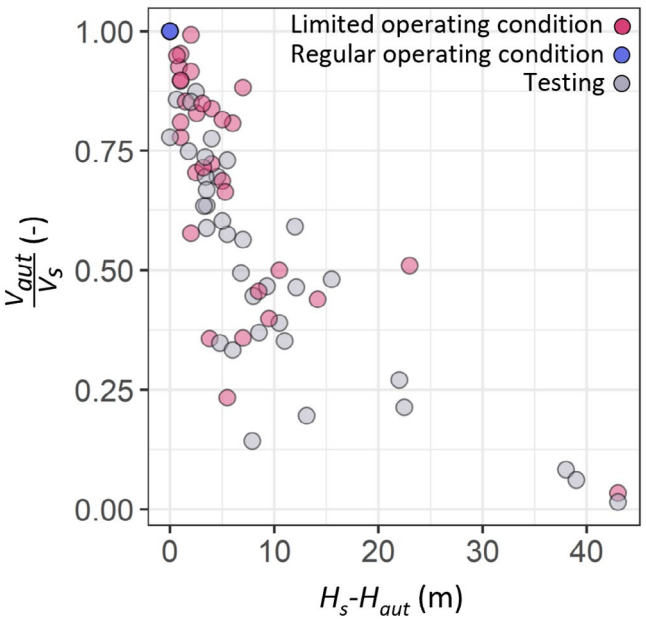



**FIGURE 3** | Percentage of authorized volume ($V_{aut}$) to total storage capacity ($V_s$) as a function of the difference between the elevation of the spillway crest ($H_s$) and the authorized water level ($H_{aut}$) for reservoirs under different operating conditions. Dot transparency reflects data point density, with lower transparency representing fewer points. The purple dot in the upper left indicates a high concentration of dams, while transparent dots represent single dams.

### 3.2 | Historical Time Series of Reservoir Storage

Daily historical observations of stored volumes were collected for 47 reservoirs located in Piedmont and Aosta Valley, in northwestern Italy, covering the period from 2006 to 2014. These data, supplied by the Italian Department of Dams, were provided in text format and were later processed for consistency and standardization. The spatial and temporal distribution of these data is presented in Figure 4. Additionally, monthly average historical observations of reservoir volumes from 1996 to 2023 were collected for 18 reservoirs in Sardinia. The data, sourced from the River Basin Document Center (*Centro di documentazione dei bacini idrografici*, CEDOC, https://www.sardegnacedoc.it/, last access: 05/05/2025), were originally presented as graphs on the website and were manually digitized for analysis. Figure 4 illustrates the spatial distribution of these data. The temporal distribution, on the other hand, is not shown, as the data are systematically available for all reservoirs uniformly from 1996 to 2023.

As shown in Figure 4a, dams in northern Italy are primarily used for hydropower generation, which follows specific regulation patterns. Reservoirs with weekly or daily regulation, for which clear seasonal patterns of reservoir storage could not be identified, have been excluded from the analysis. Similarly, very small dams, which are typically maintained at full capacity throughout the year, have not been considered. Certain specific cases were also excluded; an example is the Beauregard dam in Aosta Valley, for which the available data cover the period around 2011, when the dam's height was lowered by about 50 m. Therefore, the empirical criterion presented in Section 2.2 was defined using data from 23 dams in the Piedmont and Aosta Valley regions and 16 dams in Sardinia.

## 4 | Results

### 4.1 | Variability of the Initial Storage Levels Between Reservoirs in Northern and Southern Italy

In this section, we assess the spatial pattern of the initial storage levels (*ISLs*) for the entire sample of dams. These values are inferred from observed reservoir storage data where available, along with regional flood seasonality as shown in Figure 1. Overall, most dams have an *ISL* ranging between 0.5 and 0.9, with a peak around 0.7 (Figure 5). Very few dams have an *ISL* higher than 0.8, and no *ISL* values exceed 0.86. This suggests a potential flood control storage of around 15% for all dams. Many dams located in the Alps and northern regions show high *ISL* values, indicating that reservoirs in these areas are moderately full when major floods occur. Flooding in these areas typically occurs in late summer, when reservoirs have already partially filled due to spring snowmelt. Dams in the Eastern Alps exhibit a mix of medium to high *ISL* values, although some dams in the region have lower *ISL* values.



1753318x, 2025, 4, Downloaded from https://onlinelibrary.wiley.com/doi/10.1111/jfr3.70142 by Politecnico Di Torino Sist. Bibl Del Polit Di Torino, Wiley Online Library on [21/10/2025]. See the Terms and Conditions (https://onlinelibrary.wiley.com/terms-and-conditions) on Wiley Online Library for rules of use; OA articles are governed by the applicable Creative Commons License

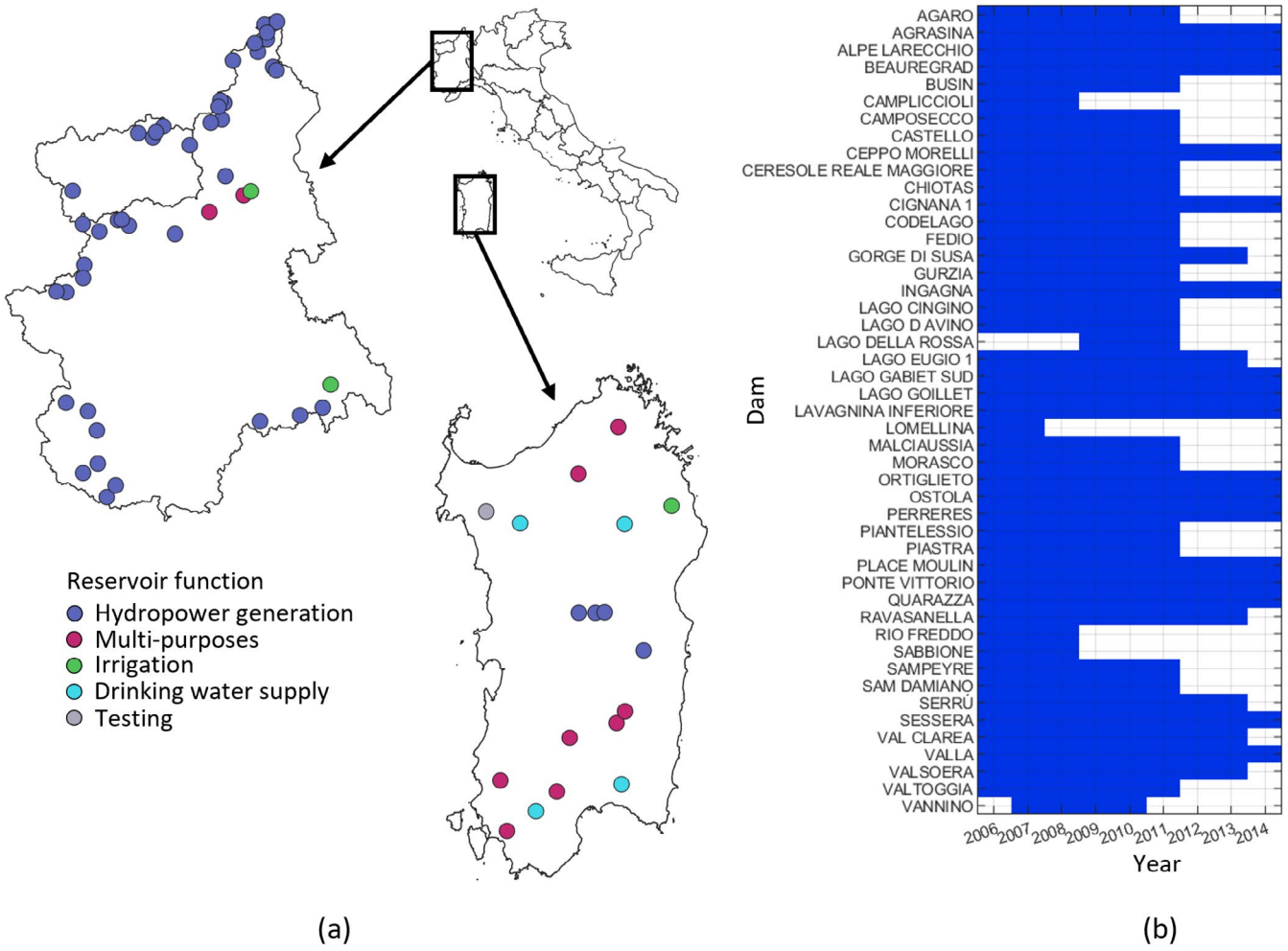



**FIGURE 4** | (a) Spatial distribution of reservoirs in Piedmont, Aosta Valley, and Sardinia with historical stored volume data, categorized by their primary reservoir function. (b) Temporal availability of data for reservoirs in Piedmont and Aosta Valley. The temporal distribution of data for Sardinia is not shown, as it is uniformly available for all reservoirs from 1996 to 2023.

To evaluate the robustness of the classification criterion adopted for dam categorization, we analyzed the monthly rainfall regimes of the catchments upstream of the dams for both dam categories: those situated in cold and wet climate zones and those in temperate and dry climate zones. Monthly precipitation data were sourced from Braca et al. (2024). Figure 6 presents the catchment-averaged mean monthly precipitation totals for the upstream watersheds of the 247 dams considered, categorized by climate zone. The analysis reveals clear seasonal differences between the two climate categories. Dams in cold, wet climate zones, typically found in the Alps, exhibit the lowest precipitation amounts during the winter months (Figure 6a), whereas dams situated in temperate, generally drier climate zones experience their lowest precipitation levels during the summer (Figure 6b). These seasonal patterns of precipitation align with those of the median storage levels for the two groups, as depicted in Figure 1b,c. Indeed, the reconstructed *MSL* reaches its lowest values during the months with minimal precipitation for both groups. Therefore, Figure 6 demonstrates that the classification approach detailed in Section 2.2, although simplified, yields a consistent grouping of rainfall regimes within each category, reinforcing the reservoir subdivision criterion used in this study and ensuring that the hydrological controls influencing reservoir storage can be effectively captured.

## 4.2 | Variability of Flood Peak Attenuation With Flood Return Periods

This section presents the results of the computation of the flood attenuation coefficients $\eta$ using a runoff coefficient of 0.5 and a seasonal-dependent *ISL*. The $\eta$-$T$ relationships were investigated and classified empirically in order to identify typical patterns. Seven groups have been found, as shown in Figure 7. Group 7, not included in Figure 7, consists of dams in which the spillway elevation is never reached; therefore, presenting consistently null $\eta$ values.

As shown in Figure 7, $\eta$ increases with the return period $T$ across all groups, indicating a worsening of the attenuation efficiency for larger floods, as expected (see e.g., Masoero et al. 2014; Volpi et al. 2018). More interestingly, the slope of the $\eta$-$T$ lines varies between groups, highlighting differences in attenuation characteristics among the classified dam categories. Within Group 1, the behavior is monotonically increasing in the semi-logarithmic plot, with only minor incremental variations, indicating a relatively constant flood mitigation efficiency across all return periods (Figure 7a). Nearly horizontal lines can be observed when $\eta$ exceeds 0.8, indicating a weaker dependence on return period when flood mitigation effectiveness is low. Conversely, dams



1753318x, 2025, 4, Downloaded from https://onlinelibrary.wiley.com/doi/10.1111/jfr3.70142 by Politecnico Di Torino Sist. Bibl Del Polit Di Torino, Wiley Online Library on [21/10/2025]. See the Terms and Conditions (https://onlinelibrary.wiley.com/terms-and-conditions) on Wiley Online Library for rules of use; OA articles are governed by the applicable Creative Commons License

within Group 2 exhibit curved lines in the semi-logarithmic plot (Figure 7c), indicating a more pronounced increase in $\eta$ with $T$ at lower return periods. Dams in both Group 3 (Figure 7e) and Group 4 (Figure 7g) exhibit a threshold behavior, in which outflow initiation occurs only once a specific return period is exceeded. The return period threshold varies depending on the dam. However, the two groups differ in the rate of increase of $\eta$ with $T$, with Group 4 showing a steeper rise compared to Group 3. A similar threshold behavior is observed for Group 6 (Figure 7k), with a very small increase in $\eta$ as $T$ increases. Finally, Group 5 consists of a small subset of dams characterized by irregular $\eta$-$T$ curves (Figure 7i). Unlike the other groups, where a clear trend or threshold effect is observed, the attenuation coefficients in Group 5 do not follow a consistent pattern.

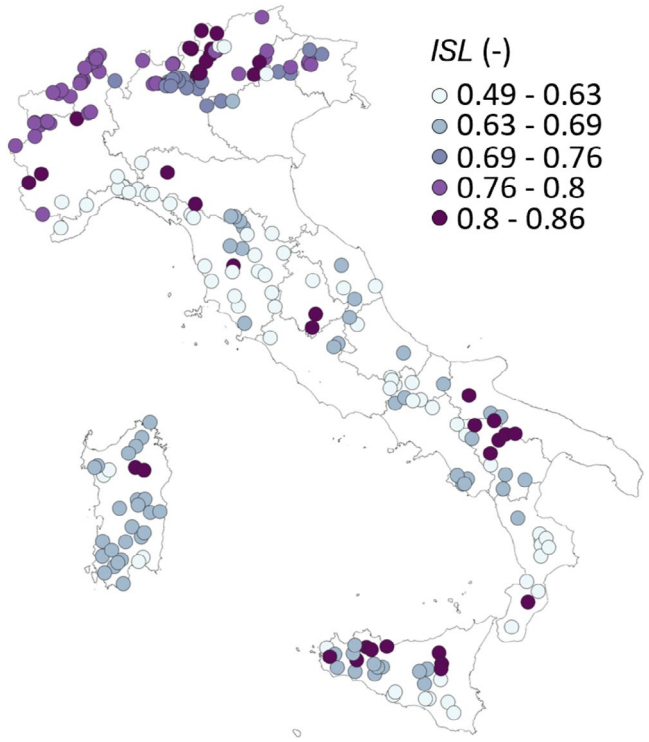



**FIGURE 5** | Spatial distribution of *ISL* values across the sample.

As shown in Figure 7, the geographical location of the dams does not seem to directly influence the classification outcomes, as dams within each group are distributed uniformly throughout the country and no specific patterns are observed. Therefore, there seems to be no direct relationship with the spatial patterns of rainfall growth curves presented in Figure 2b.

### 4.3 | Sensitivity of Flood Peak Attenuation to Different Scenarios

In this section, we present results for different scenarios of both hydrological forcings and initial reservoir conditions. Figure 8 shows the $\eta$-$T$ lines, categorized according to the classification established in the previous section, obtained when using a runoff coefficient $C=1$ and a $ISL \neq 1$. Hence, in this scenario the incoming flood peak is doubled compared to the values analyzed in the previous section. The color coding in Figure 8 is consistent with that used in Figure 7. One can observe that doubling the flood peak does not result in a proportional reduction in the dam attenuation efficiency, but rather leads to a non-linear larger decrease in attenuation efficiency as the system's limits are approached. As a result, the shape of the $\eta$–$T$ curves changes within the different classes, with several dams, regardless of their original group, displaying similar (irregular) patterns to those seen in Group 5 of Figure 7.

Figure 9 provides a comparative summary of the results across different scenarios, showing the number of dams reaching their maximum allowed water level under each condition, defined as the elevation which, when added to the dam freeboard, equals the crest elevation.

Under the scenario defined by $C=0.5$ and $ISL \neq 1$, less than 25 dams reach their maximum allowed water level. In the most conservative approach, assuming a full-lake scenario at the onset of the event, as commonly adopted for design purposes,

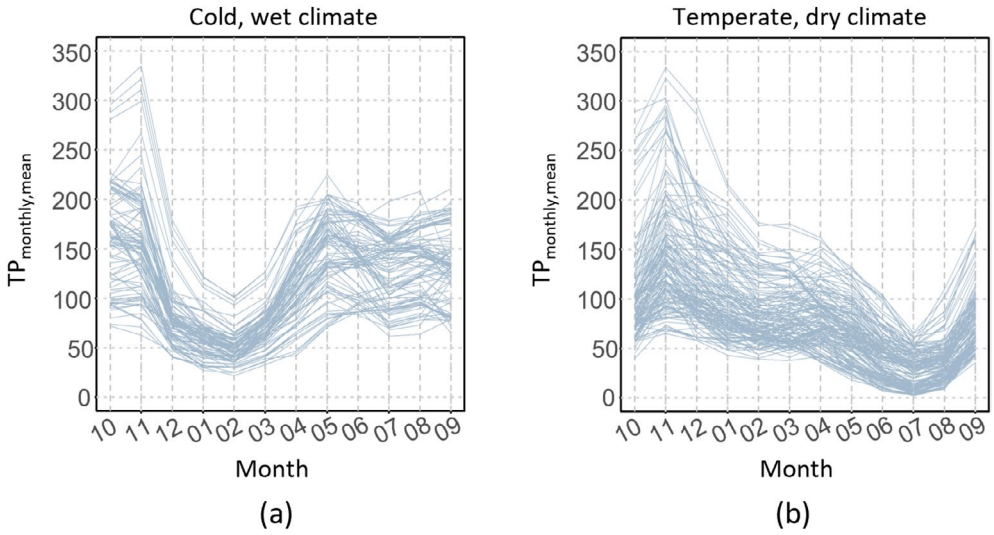



**FIGURE 6** | Catchment-averaged mean monthly precipitation totals for dams located in cold, wet climate areas (a) and temperate, dry climate areas (b).



17533180, 2025, 4, Downloaded from https://onlinelibrary.wiley.com/doi/10.1111/jfr3.70142 by Politecnico Di Torino Sist. Bibl Del Polit Di Torino, Wiley Online Library on [21/10/2025]. See the Terms and Conditions (https://onlinelibrary.wiley.com/terms-and-conditions) on Wiley Online Library for rules of use; OA articles are governed by the applicable Creative Commons License

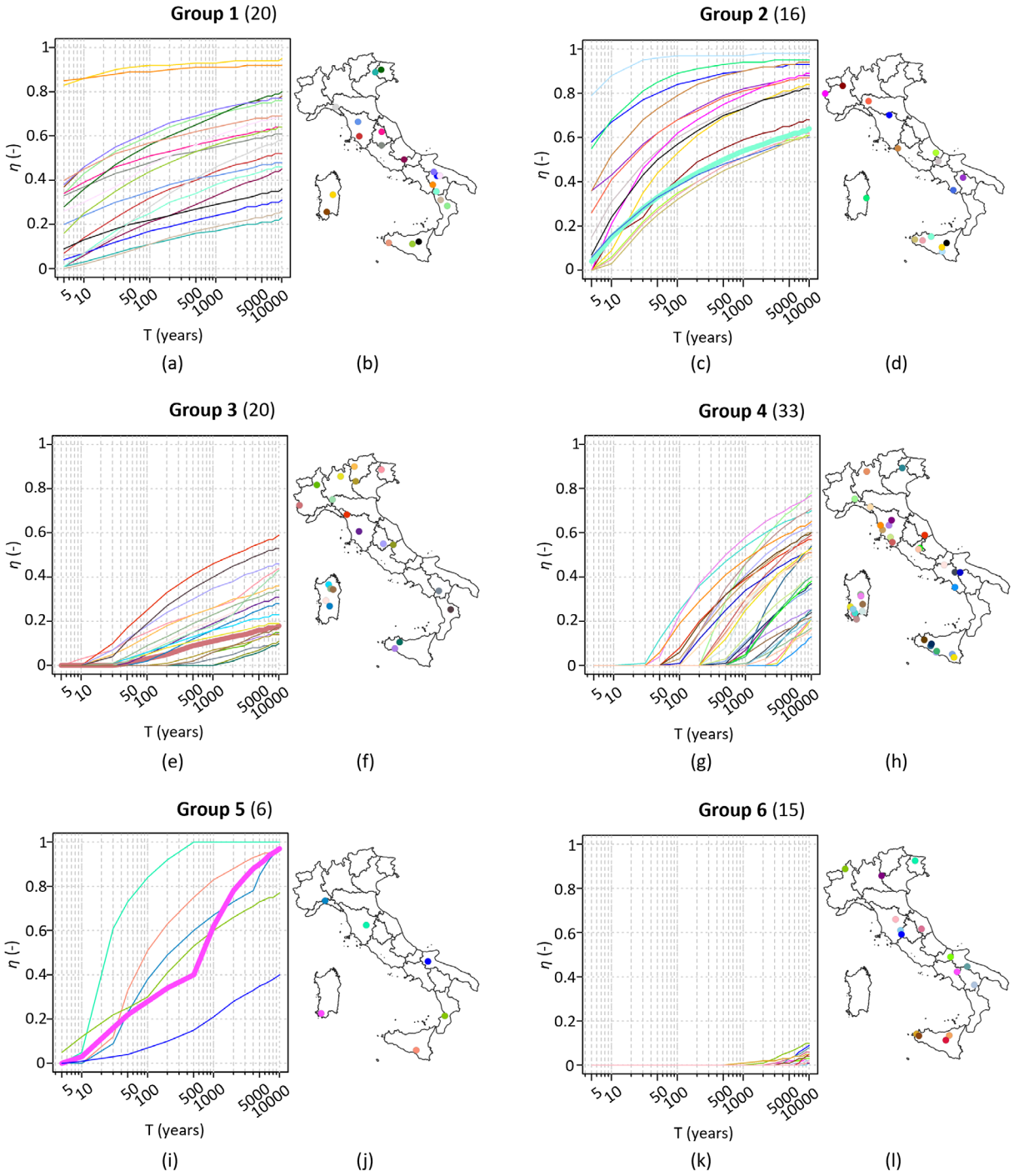



**FIGURE 7** | Attenuation coefficients $\eta$ as a function of return period $T$ for 6 of the groups identified (panels a, c, e, g, i, k). Thicker lines refer to dams selected as representative case studies, presented in detail in Appendix A. Spatial distribution of dams belonging to each group (panels b, d, f, h, j, l). A runoff coefficient $C = 0.5$ and a $ISL \neq 1$ were used to compute $\eta$. Number in brackets refer to the number of dams included in each group.

combined with a flood peak corresponding to a unit runoff coefficient, approximately 20% of the examined dams reach their maximum allowed water level for return periods of 100 years or less. A closer analysis reveals that most of these dams share a common geometric characteristic: a very small offset, typically less than or equal to 1 m, between the maximum allowed water level and the spillway crest. This configuration is found in roughly half of all large dams in Italy (Evangelista et al. 2025).

## 5 | Discussion

As previously mentioned, the attenuation effect of a dam strongly depends on the assumptions made during the analysis, including both its initial state and the applied hydrological forcing. Some considerations on reference attenuation coefficients $\eta$ for the Italian dams can be found in Evangelista et al. (2023), who selected ideal combinations of catchment characteristics and reservoir geometries with respect to the dams' flood mitigation



17533180, 2025, 4, Downloaded from https://onlinelibrary.wiley.com/doi/10.1111/jfr3.70142 by Politecnico Di Torino Sist. Bibl Del Polit Di Torino, Wiley Online Library on [21/10/2025]. See the Terms and Conditions (https://onlinelibrary.wiley.com/terms-and-conditions) on Wiley Online Library for rules of use; OA articles are governed by the applicable Creative Commons License

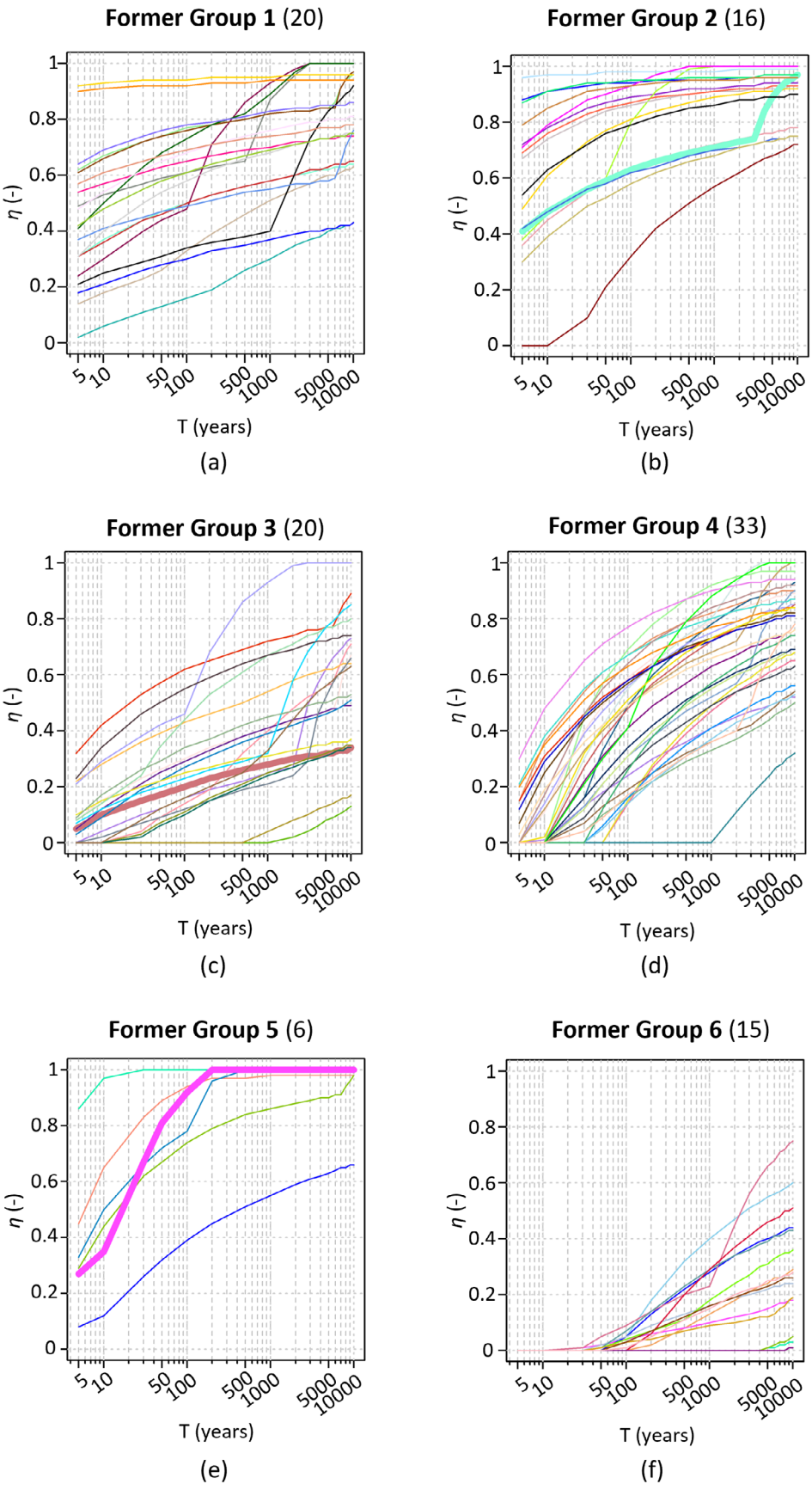



**FIGURE 8** | Attenuation coefficients $\eta$ as a function of return period $T$ for 6 of the groups identified in the previous section, i.e., Group 1 (panel a), Group 2 (panel b), Group 3 (panel c), Group 4 (panel d), Group 5 (panel e), Group 6 (panel f). Thicker lines refer to dams selected as case studies and presented in detail in Appendix A. A runoff coefficient $C=1$ and a $ISL \neq 1$ were used to compute $\eta$. Number in brackets refer to the number of dams included in each group.



1753318x, 2025, 4, Downloaded from https://onlinelibrary.wiley.com/doi/10.1111/jfr3.70142 by Politecnico Di Torino Sist. Bibl Del Polit Di Torino, Wiley Online Library on [21/10/2025]. See the Terms and Conditions (https://onlinelibrary.wiley.com/terms-and-conditions) on Wiley Online Library for rules of use; OA articles are governed by the applicable Creative Commons License

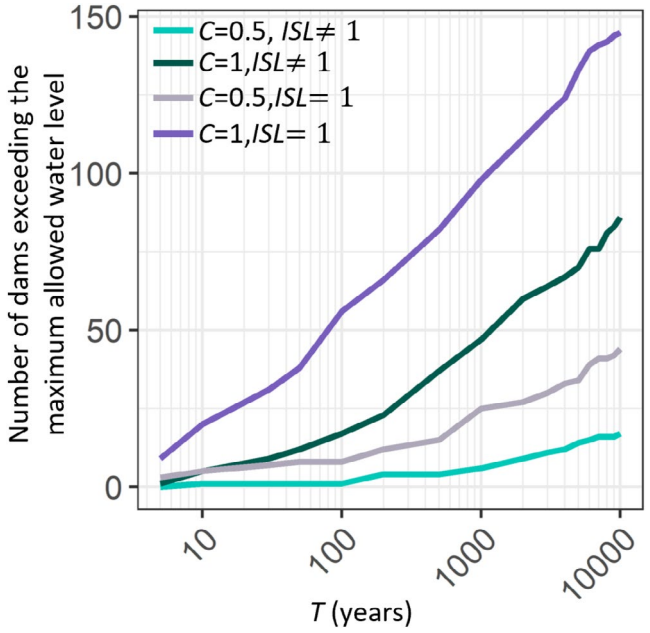



**FIGURE 9** | Number of dams reaching their maximum allowed water level as the flood return period increases, under different scenarios of hydrological forcings ($C=0.5$ or $C=1$) and initial reservoir condition ($ISL\neq1$ or $ISL=1$).

efficiency. The best combination resulted in one that is common among the Alpine dams, where high lake-to-catchment area ratios are found, coupled with high *IDF-n* parameter values and low *IDF-a* parameter values. This set of *IDF* parameters is defined by the authors as "favorable" hydrological conditions, meaning relatively low values of extreme rainfall quantiles compared to other areas.

Beyond focusing on the value of the attenuation itself, our primary interest here lies in exploring its relationship with the flood return period. $\eta$-$T$ lines for a full reservoir scenario have been analyzed for a sample of dams in north-western Italy by Masoero et al. (2014). In that study, the authors observed that the curves were generally pseudo-parallel, indicating that while the attenuation coefficient slightly increases with the return period, the overall behavior across the set of dams follows a similar pattern. In contrast, no similar analysis seems to have been conducted for a partially full reservoir scenario before the present study.

In the context of this paper, the empirical classification of $\eta$-$T$ curves that have been performed in Section 4 can be understood as a way of categorizing dams according to the return period $T$ required for the attenuation coefficient $\eta$ to approach 0. In other words, it represents the highest return period for which the reservoir can store the entire flood volume without spilling. With the exception of Group 5, as one moves from Group 1 to Group 6, the return period at which $\eta$ approaches the lowest value tends to increase. This suggests that for dams in higher-numbered groups, even large floods (in terms of their return period) can be fully attenuated by the available reservoir storage.

Figures 7 and 8 indicate that a dam's group membership is not directly determined by its geographic location. To better understand what primarily governs group classification, an analysis was conducted to identify the key structural features that differentiate one group from another. Figure 10 illustrates the relationship between the attenuation coefficients for a return period of $T=1000$ years and the ratio of a 1000-year flood volume ($V_{1000}$) to the available storage at the beginning of the routing process ($V_{av}$). The latter is computed according to Equation (7):

$$V_{av} = V_{aut} - V_{initial} \tag{7}$$

Results from the different groups are highlighted in Figure 10. Dams classified under Groups 6 and 7 (pink and purple points) are such that the entire volume of a 1000-year flood can be stored ($V_{1000}/V_{av}\leq1$). For $V_{1000}/V_{av}>1$, and again with the exception of Group 5, one can notice from Figure 10b that each group corresponds to certain ranges of the $V_{1000}/V_{av}$ ratio, as the arrangement of each group within the graph appears to follow a pattern. A dam's geographic location, therefore, doesn't directly determine its group, but rather influences the *ISL*, which in turn affects the available storage capacity ($V_{av}$) in relation to the incoming flood magnitude ($V_{1000}$).

The size of points in Figure 10b corresponds to the value of the ratio between the "storage coefficient" $k$, related to the linear reservoir equation (see below) and the basin time of concentration (referred to as $\delta$):

$$\delta = \frac{k}{t_c} \tag{8}$$

The storage coefficient $k$ is defined as the ratio between the stored volume $V_0$ for a water level of 1 m above the spillway crest, and the outgoing discharge $Q_0$ for the same water level. $k$ is expressed in hours and is computed as:

$$k = \frac{V_0}{Q_0} = \frac{A_L}{C_D W\sqrt{2g}} \tag{9}$$

where $A_L$ is the lake area, $W$ is the spillway length, $C_D$ is the discharge coefficient and $g$ is the gravity acceleration. Equation (9) exemplifies the "linear reservoir" concept (see Chow et al. 1988), as applied to a specific reference condition. The storage coefficient in Equation (9) is often used as an indicator for flood attenuation efficiency (e.g., Cipollini et al. 2022; Pirone et al. 2024): the greater the $k$ value, the greater the reservoir attenuation capacity. Being $k$ a time parameter, when divided by the basin's time of concentration, its non-dimensional value expresses a measure of the potential of the reservoir to temporally store flood volumes. Although $k$ refers to what happens once the spillway elevation is exceeded, it remains a useful discriminant in the classification framework we are performing.

As shown in Figure 10b, for a given $V_{1000}/V_{av}$ ratio, the assignment of a dam to a particular group is influenced by the corresponding $\delta$ value: for low $V_{1000}/V_{av}$ values, high $\delta$ corresponds to Group 3, while low $\delta$ corresponds to Group 4. Conversely, for high $V_{1000}/V_{av}$ values, high $\delta$ corresponds to Group 1, and low $\delta$ corresponds to Group 2.



17533186, 2025, 4, Downloaded from https://onlinelibrary.wiley.com/doi/10.1111/jfr3.70142 by Politecnico Di Torino Sist. Bibl Del Polit Di Torino, Wiley Online Library on [21/10/2025]. See the Terms and Conditions (https://onlinelibrary.wiley.com/terms-and-conditions) on Wiley Online Library for rules of use; OA articles are governed by the applicable Creative Commons License

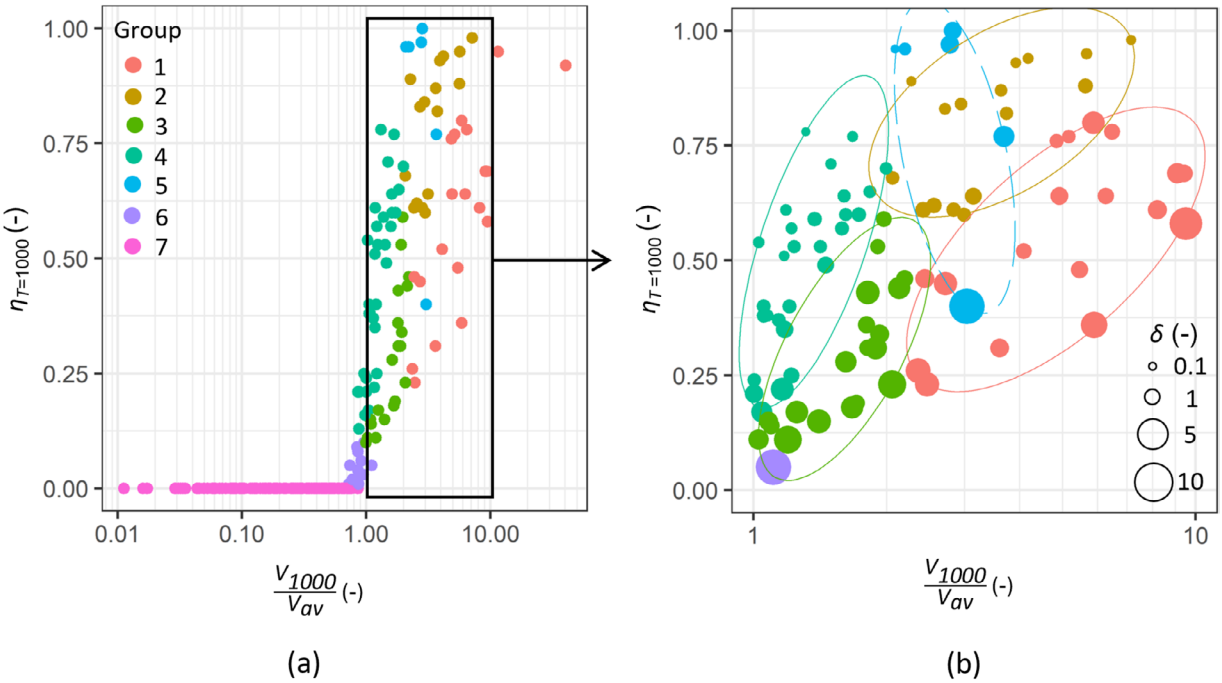



**FIGURE 10** | Relationship between the attenuation coefficient $\eta$ for a return period of $T = 1000$ years and the ratio of the 1000-year flood volume to the available storage capacity, with data points color-coded according to dam grouping (a). Zoom in on the portion of the graph for $V_{1000}/V_{av}$ values ranging from 1 to 10 (b). The ellipses plotted represent the smallest enclosing ellipses that encompass all the points within each group, while point sizes correspond to the $\delta$ value, defined as the ratio of the storage coefficient to the time of concentration (see Equations (8) and (9)).

Regarding Group 7, in which no dam produces outflow, one might ask: why are spillways not being activated in a considerable number of dams, even by large floods? To explore this point, Figure 11 shows the distribution of *ISL* values and lake-to-catchment area ratios ($A_L/A_B$) in a graph given by the values of catchment-averaged pairs ($a$, $n$) of the *IDF* curves for all the 137 dams classified within Group 7. *ISL* values are represented by point color, while point size represents $A_L/A_B$ values. This visualization builds upon the representation framework proposed in Figure 6 by Evangelista et al. (2023). Three zones can be identified in Figure 11.

i. Zone A, characterized by high *ISL* values, medium to high $A_L/A_B$ values, and favorable hydrological conditions (according to the definition provided earlier in the paper). The absence of outflow generation from dams within this area, despite medium to high *ISL* values are observed, could be attributed to the advantageous interplay of their hydrological conditions and geometric characteristics.

ii. Zone B, comprising dams with low to medium *ISL* values, small to medium $A_L/A_B$ values, and unfavorable hydrological conditions, characterized by very high $a$ values. Despite being situated in regions experiencing high rainfall amounts and having relatively small storage capacities, these dams generally do not produce overflow since they tend to have significantly low *ISL*s when flood events occur, allowing them to accommodate significant inflows.

iii. Zone C, defined by small to high *ISL* values, small to large $A_L/A_B$ values, and average hydrological conditions. The

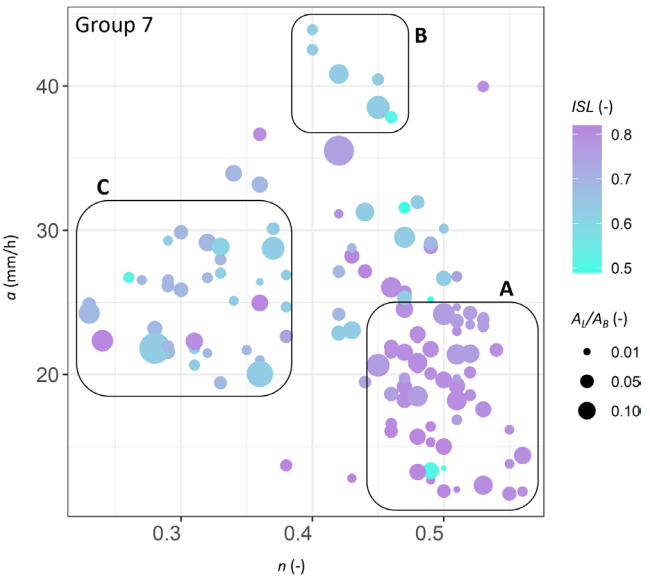



**FIGURE 11** | Range of variability of the *IDF*-parameters $a$ and $n$ for 137 dams classified within Group 7, including those that do not produce outflows. Data points are color-coded according to the initial storage level (*ISL*), while point size represents lake-to-catchment area ratio ($A_L/A_B$). Three characteristic regions are highlighted in the graph: (A) high *ISL* values, medium to high $A_L/A_B$ values, and favorable hydrological conditions; (B) low to medium *ISL* values, small to medium $A_L/A_B$ values, and unfavorable hydrological conditions; and (C) small to high *ISL* values, small to large $A_L/A_B$ values, and average hydrological conditions.



1753318x, 2025, 4, Downloaded from https://onlinelibrary.wiley.com/doi/10.1111/jfr3.70142 by Politecnico Di Torino Sist. Bibl Del Polit Di Torino, Wiley Online Library on [21/10/2025]. See the Terms and Conditions (https://onlinelibrary.wiley.com/terms-and-conditions) on Wiley Online Library for rules of use; OA articles are governed by the applicable Creative Commons License

potential of these dams to accommodate inflows without exceeding the spillway elevation could be attributed to their intermediate characteristics, which lie between the conditions observed in Zones A and B.

The findings presented in Figure 11 should also be interpreted in the context of future hydrological scenarios. Mazzoglio et al. (2025) recently documented a trend of increasing intensity in rare, high-magnitude rainfall events which is quite uniform across the Alps. This suggests that the hydrological conditions previously considered "favorable" for flood attenuation, as identified for Zone A in Figure 11, may no longer provide the same level of effectiveness in the future. Results from this study may, in this sense, inform future assessments of reservoir management strategies.

## 6 | Conclusions

Large reservoirs in Italy are often operated below their maximum capacity. This is due to climatic-hydrological conditions and to operational factors. This study emphasizes the critical role of the initial reservoir storage in influencing flood attenuation effects. Specifically, we have investigated how the attenuation efficiency of approximately 250 large dams across Italy, for which an initial storage level was reconstructed based on flood seasonality, varies across a range of flood events, from very small floods to those with return periods exceeding 1000 years.

The main contributions of this study can be outlined as follows:

i. Variability of flood attenuation efficiency with flood severity: the reduction in peak discharge is neither spatially homogeneous nor uniform with increasing flood return periods $T$ when initial storage levels are reduced. This relationship is strongly non-linear; for instance, as the reservoir reaches its capacity limits, doubling the incoming flood peak leads to abrupt reductions in attenuation efficiency.

ii. Classification of dams according to their attenuation behavior: based on the initially available storage capacity for flood control and the actual reservoir geometries, dams were classified according to the flood severity level needed to cause a significant reduction in their attenuation capacity. This classification allows us to distinguish between dams that experience a gradual decline in performance with increasing flood return periods and those that undergo a threshold effect.

iii. Overly conservative estimates under full-reservoir assumptions: considering reservoirs to be at maximum capacity, a common practice in dam safety assessments, combined with conservative flood peak estimates, that is, obtained with a runoff coefficient of 1, tends to produce overly cautious outcomes. Under this scenario, around 50 dams reach their maximum allowed water level for flood return periods of 100 years or less, which would seem rather unlikely in practice, considering typical spillway design standards.

Although suitable for capturing all these aspects, the methodology applied here is based on some assumptions that deserve attention. First, the approach used for estimating the initial storage level is data-driven and does not account for the joint probability distribution between flood timing (seasonality) and the seasonal variation in reservoir storage levels. Second, the seasonal variability of the initial storage levels (shown in Figure 1) is simplified, as it primarily depends on the dam's elevation and the regional climatology. While this implicitly accounts for different reservoir uses (e.g., irrigation dams are typically not located at high elevations), fluctuations in reservoir levels driven by the primary purpose of the dam are not explicitly considered in the analysis. Despite the simplifications adopted in this study, the results align reasonably well with the actual conditions of dams in Italy, as further exemplified by the detailed analysis of three case studies presented in Appendix A.

The conclusions drawn present relevant practical implications for the national-scale focus of this study. When analyzing different reservoirs, a dam that might initially appear more efficient than others may not be as effective overall, once the initial reservoir storage is factored into the analysis, due to possible strong nonlinearity of the $\eta$-$T$ curve. Such indications, together with the effects of reservoir geometry on the dam efficiency, may provide guidance for stakeholders and dam operators, particularly in the context of climate change and future flood risk management.


### Acknowledgments

The authors wish to thank the Italian Department of Dams and Hydroelectrical Infrastructure for sharing data. This study was carried out within the RETURN Extended Partnership and received funding from the European Union Next-GenerationEU (National Recovery and Resilience Plan—NRRP, Mission 4, Component 2, Investment 1.3-D.D. 1243 2/8/2022, PE0000005-Spoke TS 2). Open access publishing facilitated by Politecnico di Torino, as part of the Wiley - CRUI-CARE agreement.


### Conflicts of Interest

The authors declare no conflicts of interest.

### Data Availability Statement

The majority of the data supporting the findings of this study are available in TILDE (The Italian Large Dams datasEt, Evangelista et al. 2025). Additional data can be obtained from the corresponding author upon request.

### References


Antolini, F., and E. Tate. 2021. "Location Matters: A Framework to Investigate the Spatial Characteristics of Distributed Flood Attenuation." *Water (Basel)* 13, no. 19: 2706. https://doi.org/10.3390/w13192706.

Bai, X., W. Liu, T. Wang, et al. 2024. "Large-Sample Detection of Reservoir Impacts on Flow Regime Alteration Through Improved Paired-Catchment Approach." *Journal of Hydrology* 642: 131872. https://doi.org/10.1016/j.jhydrol.2024.131872.

Beck, H. E., T. R. McVicar, N. Vergopolan, et al. 2023. "High-Resolution (1 Km) Köppen-Geiger Maps for 1901–2099 Based on Constrained CMIP6 Projections." *Scientific Data* 10: 724. https://doi.org/10.1038/s41597-023-02549-6.

Blöschl, G., J. Hall, J. Parajka, et al. 2017. "Changing Climate Shifts Timing of European Floods." *Science* 357: 588–590. https://doi.org/10.1126/science.aan2506.





17533180, 2025, 4, Downloaded from https://onlinelibrary.wiley.com/doi/10.1111/jfr3.70142 by Politecnico Di Torino Sist. Bibl Del Polit Di Torino, Wiley Online Library on [21/10/2025]. See the Terms and Conditions (https://onlinelibrary.wiley.com/terms-and-conditions) on Wiley Online Library for rules of use; OA articles are governed by the applicable Creative Commons License

Braca, G., M. Bussettini, B. Lastoria, S. Mariani, and F. Piva. 2024. "Elaborazioni Modello BIGBANG Versione 8.0, Istituto Superiore per la Protezione e la Ricerca Ambientale—ISPRA [Dataset]." https://groupware.sinanet.isprambiente.it/bigbang-data/library/bigbang_80/.

Brigandì, G., A. Candela, and G. T. Aronica. 2023. "Analysis of the Effects of Reservoir Operating Scenarios on Downstream Flood Damage Risk Using an Integrated Monte Carlo Modelling Approach." *Water (Basel)* 15, no. 3: 550. https://doi.org/10.3390/w15030550.

Brunner, M. 2021. "Reservoir Regulation Affects Droughts and Floods at Local and Regional Scales." *Environmental Research Letters* 16: 124016. https://doi.org/10.1088/1748-9326/ac36f6.

Brunner, M. I., and P. Naveau. 2023. "Spatial Variability in Alpine Reservoir Regulation: Deriving Reservoir Operations From Streamflow Using Generalized Additive Models." *Hydrology and Earth System Sciences* 27: 673–687. https://doi.org/10.5194/hess-27-673-2023.

Carvajal, C., L. Peyras, P. Arnaud, D. Boissier, and P. Royet. 2009. "Probabilistic Modeling of Floodwater Level for Dam Reservoirs." *Journal of Hydrologic Engineering* 14, no. 3: 223–232. https://doi.org/10.1061/(ASCE)1084-0699(2009)14:3(223).

Chow, V. T., D. R. Maidment, and L. W. Mays. 1988. *Applied Hydrology*. McGraw-Hill Book Company.

Cipollini, S., A. Fiori, and E. Volpi. 2022. "A New Physically Based Index to Quantify the Impact of Multiple Reservoirs on Flood Frequency at the Catchment Scale Based on the Concept of Equivalent Reservoir." *Water Resources Research* 58: e2021WR031470. https://doi.org/10.1029/2021WR031470.

Evangelista, G., D. Ganora, P. Mazzoglio, F. Pianigiani, and P. Claps. 2023. "Flood Attenuation Potential of Italian Dams: Sensitivity on Geomorphic and Climatological Factors." *Water Resources Management* 37, no. 15: 6165–6181. https://doi.org/10.1007/s11269-023-03649-z.

Evangelista, G., P. Mazzoglio, D. Ganora, F. Pianigiani, and P. Claps. 2025. "Features of Italian Large Dams and Their Upstream Catchments." *Earth System Science Data* 17: 1407–1426. https://doi.org/10.5194/essd-17-1407-2025.

Evangelista, G., R. Woods, and P. Claps. 2024. "Towards Robust Operational Estimation of the Time of Concentration in Ungauged Basins." Atti del XXXIX Convegno Nazionale di Idraulica e Costruzioni Idrauliche, Italy.

Federal Emergency Management Agency (FEMA). 2012. "Summary of Existing Guidelines for Hydrologic Safety of Dams (FEMA P-919), US Department of Homeland Security." https://damfailures.org/wp-content/uploads/2018/09/01_hydrosafetydam_intro.pdf.

Fluixá-Sanmartín, J., L. Altarejos-García, A. Morales-Torres, and I. Escuder-Bueno. 2018. "Review Article: Climate Change Impacts on Dam Safety." *Natural Hazards and Earth System Sciences* 18: 2471–2488. https://doi.org/10.5194/nhess-18-2471-2018.

Gabriel-Martin, I., A. Sordo-Ward, L. Garrote, and L. G. Castillo. 2017. "Influence of Initial Reservoir Level and Gate Failure in Dam Safety Analysis. Stochastic Approach." *Journal of Hydrology* 550: 669–684. https://doi.org/10.1016/j.jhydrol.2017.05.032.

Gabriel-Martin, I., A. Sordo-Ward, L. Garrote, and I. Granados. 2019. "Hydrological Risk Analysis of Dams: The Influence of Initial Reservoir Level Conditions." *Water (Basel)* 11, no. 3: 461. https://doi.org/10.3390/w11030461.

Hall, J., B. Arheimer, M. Borga, et al. 2014. "Understanding Flood Regime Changes in Europe: A State-Of-The-Art Assessment." *Hydrology and Earth System Sciences* 18: 2735–2772. https://doi.org/10.5194/hess-18-2735-2014.

Liuzzo, L., L. V. Noto, E. Arnone, D. Caracciolo, and G. La Loggia. 2015. "Modifications in Water Resources Availability Under Climate Changes: A Case Study in a Sicilian Basin." *Water Resources Management* 29: 1117–1135. https://doi.org/10.1007/s11269-014-0864-z.

Lompi, M., L. Mediero, E. Soriano, and E. Caporali. 2023. "Climate Change and Hydrological Dam Safety: A Stochastic Methodology Based on Climate Projections." *Hydrological Sciences Journal* 68, no. 6: 745–763. https://doi.org/10.1080/02626667.2023.2192873.

Lu, Q., P. Zhong, B. Xu, et al. 2022. "Multi-Objective Risk Analysis for Flood Control Operation of a Complex Reservoir System Under Multiple Time-Space Correlated Uncertainties." *Journal of Hydrology* 606: 127419. https://doi.org/10.1016/j.jhydrol.2021.127419.

Manfreda, S., D. Miglino, and C. Albertini. 2021. "Impact of Detention Dams on the Probability Distribution of Floods." *Hydrology and Earth System Sciences* 25: 4231–4242. https://doi.org/10.5194/hess-25-4231-2021.

Masoero, A., D. Ganora, P. Claps, and A. Petaccia. 2014. "Effects of Reservoirs on Downstream Flood Frequency Curves." Proceedings of the 3rd IAHR Europe Congress, Portugal.

Mazzoglio, P., A. Viglione, D. Ganora, and P. Claps. 2025. "Mapping the Uneven Temporal Changes in Ordinary and Extraordinary Rainfall Extremes in Italy." *Journal of Hydrology: Regional Studies* 58: 102287. https://doi.org/10.1016/j.ejrh.2025.102287.

Micovic, Z., D. N. D. Hartford, M. G. Schaefer, and B. L. Barker. 2016. "A Non-Traditional Approach to the Analysis of Flood Hazard for Dams." *Stochastic Environmental Research and Risk Assessment* 30: 559–581. https://doi.org/10.1007/s00477-015-1052-2.

Natural Environment Research Council (NERC). 1975. "Estimation of Flood Volumes Over Different Duration." in Natural Environment Research Council, Flood Studies Report. 352–373.

Peres, D. J., R. Modica, and A. Cancelliere. 2019. "Assessing Future Impacts of Climate Change on Water Supply System Performance: Application to the Pozzillo Reservoir in Sicily, Italy." *Water* 11, no. 12: 2531. https://doi.org/10.3390/w11122531.

Pirone, D., L. Cimorelli, and D. Pianese. 2024. "The Effect of Flood-Mitigation Reservoir Configuration on Peak-Discharge Reduction During Preliminary Design." *Journal of Hydrology: Regional Studies* 52: 101676. https://doi.org/10.1016/j.ejrh.2024.101676.

Salwey, S., G. Coxon, F. Pianosi, M. B. Singer, and C. Hutton. 2023. "National-Scale Detection of Reservoir Impacts Through Hydrological Signatures." *Water Resources Research* 59, no. 5: e2022WR033893. https://doi.org/10.1029/2022WR033893.

Sordo-Ward, A., L. Garrote, F. Martín-Carrasco, and M. D. Bejarano. 2012. "Extreme Flood Abatement in Large Dams With Fixed-Crest Spillways." *Journal of Hydrology* 466: 60–72. https://doi.org/10.1016/j.jhydrol.2012.08.009.

Stecher, G., and M. Herrnegger. 2022. "Impact of Hydropower Reservoirs on Floods: Evidence From Large River Basins in Austria." *Hydrological Sciences Journal* 67, no. 14: 2082–2099. https://doi.org/10.1080/02626667.2022.2130332.

Volpi, E., M. Di Lazzaro, M. Bertola, A. Viglione, and A. Fiori. 2018. "Reservoir Effect on Flood Peak Discharge at the Catchment Scale." *Water Resources Research* 54: 8623–9636. https://doi.org/10.1029/2018WR023866.

Wang, W., H. Li, L. R. Leung, et al. 2017. "Nonlinear Filtering Effects of Reservoirs on Flood Frequency Curves at the Regional Scale." *Water Resources Research* 53: 8277–8292. https://doi.org/10.1002/2017WR020871.

Watt, W. E., and K. C. A. Chow. 1985. "A General Expression for Basin Lag Lime." *Canadian Journal of Civil Engineering* 12: 294–300.

Zhao, G., P. Bates, and J. Neal. 2020. "The Impact of Dams on Design Floods in the Conterminous US." *Water Resources Research* 56: e2019WR025380. https://doi.org/10.1029/2019WR025380.



17533180, 2025, 4, Downloaded from https://onlinelibrary.wiley.com/doi/10.1111/jfr3.70142 by Politecnico Di Torino Sist. Bibl Del Polit Di Torino, Wiley Online Library on [21/10/2025]. See the Terms and Conditions (https://onlinelibrary.wiley.com/terms-and-conditions) on Wiley Online Library for rules of use; OA articles are governed by the applicable Creative Commons License

## Appendix A

### Analysis of Selected Representative Dams

This section provides some detailed considerations for three representative dams, each selected from one of the seven groups identified in Section 4.2. Figure A1 provides their locations in Italy, along with photographs showcasing construction details and views of the reservoirs. Two of them, the Rosamarina and Castello dams, are classified as major dams in Italy, as listed on the website of the Italian Department of Dams and Hydroelectrical Infrastructures (https://dgdighe.mit.gov.it/categoria/_dighe_di_rilievo, last access: 05/05/2025). The Monte Pranu Dam, representative of Group 5, was chosen as a key example of the exceedance of the maximum allowed water level.

### The Rosamarina Dam—Group 2

The Rosamarina dam is an arch-gravity structure on the San Leonardo River, located near the town of Caccamo in the province of Palermo, Sicily, and it is the largest reservoir in the western part of the region (Figure A1a). The upstream catchment area is about 500 km$^2$ while the lake area, measured at the elevation of the spillway crest, covers almost 5 km$^2$. Originally designed to meet irrigation needs, the dam

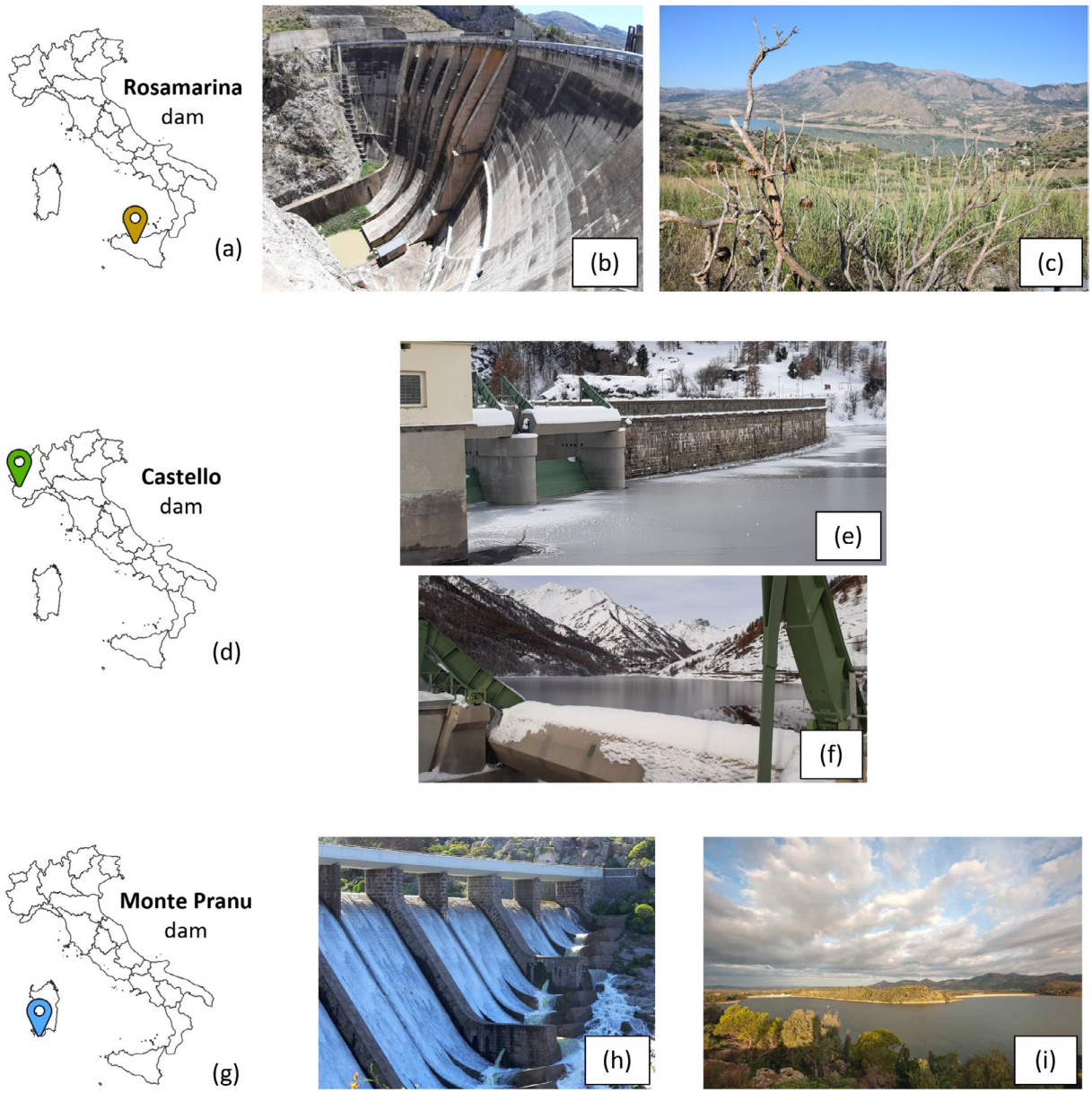



**FIGURE A1** | Dams selected as examples for more detailed considerations. Position of the Rosamarina dam (Sicily region) (a). Dam structure, spillway, and energy dissipation basin (*source:* Italian Department of Dams and Hydroelectrical Infrastructures, https://dgdighe.mit.gov.it/categoria/articolo/_dighe_di_rilievo/diga_di_rosamarina) (b). Rosamarina lake (*source:* Italian Department of Dams and Hydroelectrical Infrastructures, https://dgdighe.mit.gov.it/categoria/articolo/_dighe_di_rilievo/diga_di_rosamarina) (c). Position of the Castello dam (Piedmont region) (d). Radial gate-controlled spillway (*source:* Italian Department of Dams and Hydroelectrical Infrastructures, https://dgdighe.mit.gov.it/categoria/articolo/_dighe_di_rilievo/diga_di_castello) (e). Castello lake (*source:* Italian Department of Dams and Hydroelectrical Infrastructures, https://dgdighe.mit.gov.it/categoria/articolo/_dighe_di_rilievo/diga_di_castello) (f). Position of the Monte Pranu dam (Sardinia region) (g). Spillway (*source:* Wikipedia, https://it.wikipedia.org/wiki/Diga_di_Monte_Pranu) (h). Monte Pranu lake (*source:* Ente Acque della Sardegna, https://www.enas.sardegna.it/il-sistema-idrico-multisettoriale/laghi-artificiali/monte-pranu.html) (i).



1753318x, 2025, 4, Downloaded from https://onlinelibrary.wiley.com/doi/10.1111/jfr3.70142 by Politecnico Di Torino Sist. Bibl Del Polit Di Torino, Wiley Online Library on [21/10/2025]. See the Terms and Conditions (https://onlinelibrary.wiley.com/terms-and-conditions) on Wiley Online Library for rules of use; OA articles are governed by the applicable Creative Commons License

is currently undergoing testing. Today, its reservoir primarily supplies water for irrigation and drinking purposes, with only a small percentage allocated for hydropower. Standing 84 meters tall, the dam can hold up to 100 million cubic meters of water at full capacity, though the currently authorized limit is 73 million cubic meters. As shown in Figure A1c, its spillway system consists of six free spillways, each 12 meters long, capable of releasing a discharge of up to 1935 $m^3/s$ when the maximum allowed water level is reached.

Based on our results, when routing flood hydrographs calculated using a runoff coefficient of 0.5 and considering an *ISL* equal to 0.82, the $\eta$-$T$ line exhibits a pronounced curvature in the semi-logarithmic graph (thick teal curve in Figure 7c). The $\eta$ values range from a minimum of just over 0.1 to a maximum of approximately 0.6, corresponding to input flood peaks that vary from 430 $m^3/s$ to about 1700 $m^3/s$. Under a full-reservoir assumption ($ISL = 1$), the same hydrological forcings would have caused $\eta$ to vary much less, ranging from a minimum of 0.6 to a maximum of 0.75.

When doubling the incoming flood peaks with $ISL = 0.82$, the $\eta$-$T$ curve undergoes a sudden increase for very high return periods ($T > 1000$ years) (thick teal curve in Figure 8b), indicating that the system's capacity limit has been reached.

### The Castello Dam—Group 3

The dam, located at approximately 1500 m a.s.l., crosses the Varaita di Chianale stream near the village of Castello, in the province of Cuneo, Piedmont (Figure A1d). It is primarily used for hydropower production and regulates a catchment area of about 67 $km^2$. With a height of 70 meters and an authorized storage capacity of around 11 $Mm^3$ under regular operating conditions, the dam is equipped with two radial-gated spillways, with a total length of 21 meters (Figure A1e). The reservoir surface area is 0.6 $km^2$. This geometric configuration is quite representative of those commonly found among large Alpine dams.

Incoming flood peaks computed using a $C = 0.5$ range from 90 $m^3/s$ to approximately 300 $m^3/s$, with a maximum discharge capacity of 226 $m^3/s$ for the spillways. Although the dam is initially considered to be moderately full (with its *ISL* estimated at around 0.8), it exhibits notably high efficiency: overflow begins for return periods exceeding 50 years, and the $\eta$-$T$ line maintains a very gentle slope thereafter (thick pinkish curve in Figure 7e), indicating consistently low $\eta$ values even for very high return periods. Doubling the peak flood input causes the entire $\eta$-$T$ line to shift upwards (thick pinkish curve in Figure 8c). In this scenario, overflow occurs at very low return periods, but the line's slope remains constant, suggesting that the system does not reach its capacity limit. Even under an initially full-reservoir condition ($ISL = 1$), the system remains well below its capacity limit, with $\eta$-$T$ lines maintaining moderate slopes and maximum $\eta$ values of 0.36 and 0.44 for the $C = 0.5$ and $C = 1$ scenarios, respectively.

These results seem to align with the current situation of the dam: indeed, the Turin Technical Office for Dams, a regional branch of the Italian Department of Dams responsible for supervising large dams in Piedmont, Aosta Valley, and parts of Liguria and Lombardy, has identified the Castello dam as playing a role in mitigating downstream damage during certain flood events, particularly in the areas immediately downstream.

### The Monte Pranu Dam—Group 5

The Monte Pranu Dam impounds the Palmas Stream in the municipality of Tratalias, located in the province of South Sardinia. Originally designed for irrigation and flood mitigation of the Rio Palmas, the reservoir now serves multiple purposes, including industrial and drinking water supply. There are no current storage limitations in the management of the Monte Pranu Dam. The reservoir has a total capacity of 50 million cubic meters and was created through the construction of the main Monte Pranu stone masonry dam, along with three smaller auxiliary dams. The upstream basin covers an area of approximately 450 $km^2$. The spillway consists of eight free spillways (Figure A1h), each 8.5 meters in length, with a discharge capacity of 450 $m^3/s$ when the reservoir is at its maximum allowed water level of 45.5 m a.s.l.

According to our results, this dam belongs to Group 5 (thick pink curves in Figures 7i and 8e). Our findings indicate that, with a runoff coefficient of 0.5 and an *ISL* of 0.7, and operating with spillways only, it is not possible to manage all the considered events without resulting in overcoming the crest elevation. The dam would be overtopped by a 500-year flood, while the maximum allowed water level would be reached by a 200-year flood. Under the same hydrological forcings, if the reservoir were at full capacity at the time of the flood's arrival ($ISL = 1$), the maximum allowed level could be exceeded even during a 10-year flood event. In this scenario, for any return period, the required storage volume would exceed the available capacity of the Monte Pranu reservoir between the spillway elevation and the maximum allowable water level, which is 19.5 $mm^3$.

Over the years, the reservoir has reached full capacity multiple times, notably in November 2018 and December 2019. One significant event occurred in April 2009, when heavy rainfall caused the reservoir to exceed its storage capacity, leading to the release of excess water. This overflow caused flooding in the surrounding areas, prompting intervention by provincial engineers to manage the emergency and mitigate further impacts.

In recent years, a critical hydraulic issue has been identified regarding the discharge capacity of the spillways. As a result, the Sardinia Region has allocated significant investments to make adjustments to the spillway structures of the Monte Pranu dam to meet the requirements of the hydrological reassessments of dam safety (information available at: https://osservacantieri.mit.gov.it/cantiere/?id=29, last access: 05/05/2025).



1753318x, 2025, 4, Downloaded from https://onlinelibrary.wiley.com/doi/10.1111/jfr3.70142 by Politecnico Di Torino Sist. Bibl Del Polit Di Torino, Wiley Online Library on [21/10/2025]. See the Terms and Conditions (https://onlinelibrary.wiley.com/terms-and-conditions) on Wiley Online Library for rules of use; OA articles are governed by the applicable Creative Commons License